Proceedings of Engineering and Technology Innovation, vol. 30, 2025, pp. 11-23

Harmonic Elimination Method for Permanent Magnet Synchronous Motor Utilizing Active Disturbance Rejection Control

Marwan Kanaan Ismael[1], Saif Talal Bahar[2,*], Ahmed Aizaldeen Abdullah[2]

[1]Department of Renewable Energy Techniques, Baquba Technical Institute, Middle Technical University, Baghdad, Iraq

[2]Department of Electromechanical Techniques, Baquba Technical College, Middle Technical University, Baghdad, Iraq

Received 11 October 2024; received in revised form 10 February 2025; accepted 12 February 2025

DOI: https://doi.org/10.46604/peti.2024.14386

Abstract

This study investigates the control of permanent magnet synchronous motor (PMSM) as the core component of speed control systems. The extensive employment of PMSMs in electric cars is ascribed to their efficiency, simplicity, dependability, and stable performance. Therefore, this article suggests an active disturbance rejection control (ADRC) strategy for electric motor control systems to improve the system's robustness, accelerate response speed, and enhance tracking performance. The implementation of ADRC reduces the speed response time from 0.14 s to 0.04 s and the three-phase current drop time from 0.03 s to 0.01 s. The total harmonic distortion (THD) under the existing proportional-integral (PI) speed controller and the suggested ADRC speed controller are 10.58% and 5.73%, respectively, with the proposed ADRC having a reduced THD.

Keywords: active disturbance rejection control, THD, PI controllers, current error, PMSM

1. Introduction

Permanent magnet synchronous motors (PMSMs) are widely used in computer numerical control (CNC) machine tools, electric transmission, aerospace, and other applications due to their excellent efficiency, power density, air gap flux, and simple control structure. However, due to nonlinear factors such as the distribution of motor windings, slot effect, and inverter dead zone effect, the motor stator winding current generates harmonics, causing the motor to rotate slowly. In addition to the slow rotation, the torque and speed fluctuate, increasing motor losses and affecting the stability of its operation.

The types of harmonics in the stator winding current of PMSM are divided into two categories: time harmonics and space harmonics [1]. Specifically, time harmonics are caused by nonlinear factors of the inverter, such as the dead zone effect and switch tube voltage drop, whereas space harmonics are caused by motor structure, such as winding distribution form, magnetic circuit saturation effect, etc. In response to the problem of harmonics in the stator current of motors, domestic and foreign scholars mainly conduct research on harmonic suppression from two aspects. The first aspect is to start with the motor control strategy and use the harmonic compensation strategy to suppress harmonics. The main suppression strategies include harmonic voltage compensation, multi-rotation proportional-integral (PI) control [2], complex vector control [3], repetitive control [4-5], anti-disturbance control [6], and proportional resonance control [7].

The second aspect is to start from the motor body structure, such as the skew slot [8], and optimize the permanent magnet shape, magnetic circuit, and stator winding type to achieve current harmonic suppression. Harmonic voltage injection is the most frequently used harmonic suppression strategy. The main problem with harmonic voltage injection is detecting harmonic

* Corresponding author. E-mail address: saif.talal@mtu.edu.iq

current because the traditional PI controller can only track the AC quantity with error [8]. Therefore, the extraction of AC signals is typically considered from two perspectives. One method is to treat the harmonic as a DC quantity in the corresponding rotating coordinate system, convert the harmonic AC component into a DC component through coordinate transformation, and then obtain the harmonic DC component via a low-pass filter. The other method is to extract the harmonic AC quantity using a controller capable tracking AC signal, combined with a PI controller.

Multi-rotation coordinate transformation to extract the DC component of harmonic current [9]. Its main principle is to transform the harmonic to be suppressed into the d-q coordinate system of the corresponding order, convert the AC harmonic component into a DC harmonic component, and finally extract the harmonic compensation amount through a low-pass filter [10]. However, due to the addition of multiple PI controllers, the algorithm of this method is complex, and the parameter setting is challenging. A method is proposed, based on the relationship between the error voltage and the motor phase current polarity, aiming to compensate for the impact of inverter dead time and suppress the harmonics caused by the dead time effect. However, due to the influence of the zero-current clamping phenomenon, the polarity of the motor phase current cannot be accurately determined, which reduces the compensation accuracy and affects the inhibitory effect.

In the digital linear interpolation method, the filter approximates the fractional-order delay link, thereby enabling repetitive control. The controller's resonant frequency matches the motor current's harmonic frequency [11]. It improves the repetitive controller's ability to suppress current harmonics but suppresses the effect, which is affected by the active disturbance rejection control (ADRC) and the accuracy of the linear interpolation method. Meanwhile, a piezoelectric-order wide-angle model is proposed based on repeated control of internal models [12]. The piqued generalized integral defines the integrator's harmonic detection structure. The repetitive control internal mode is embedded in the converter to produce the fundamental wave and other sub-harmonic bands. Subsequently, the gain is generated to obtain harmonic signals of a specific sub-frequency, which is suitable for applications and has reference significance for motor harmonic detection. Concerning traditional PI controllers, the problem lies in the inability to track AC signals appropriately.

The main gap of this article is the ADRC strategy for electric motor control systems to improve the system's robustness, accelerate the response speed, and enhance the tracking performance. The ADRC strategy enhanced the system's tracking performance and response speed compared to the PI control strategy. The motor current waveform was improved, and the motor harmonic current was effectively suppressed. Moreover, the model results confirm the effectiveness of the proposed algorithm.

The article is divided into several sections: Section 1 is an introduction, Section 2 describes the engine model, Section 3 explains the concept of the traditional and improved methods and shows their forms, Section 4 presents the design of the equations for ADRC, Section 5 discusses and compares the results using tables, and Section 6 concludes the article.

2. Modelling of PMSM

To simplify the analysis, the three-phase PMSM is assumed to be an ideal motor under the following conditions. First, the permeation of the motor core is neglected. Second, the eddy current and hysteresis losses in the motor are neglected. Third, the stator current is a three-phase balanced sinusoidal current. Fourth, the conductivity of the rotor permanent magnet material is assumed to be zero. Finally, there is no damping winding on the rotor. Therefore, the stator voltage equation of the three-phase PMSM in the d-q coordinate system is given as:

$$v_d = R \times i_d + L_d \times \frac{di_d}{dt} - L_d \times \omega_e \times i_d \tag{1}$$

$$v_q = R \times i_q + L_q \times \frac{di_q}{dt} - L_q \times \omega_e \times i_d + \omega_e \times \varphi_f \tag{2}$$

where v_d and v_q are the d-axis and q-axis components of the stator voltage; i_d and i_q are the d-axis and q-axis components of the stator current; R is the stator resistance; φ_f is the permanent magnet flux; $L_d = L_q$ are the d-axis and q-axis inductances; and ω_e is the electrical angular velocity. Accordingly, the electromagnetic torque can be expressed as:

$$T_e = \frac{3}{2} \times i_q \times p \times \left(L_d - L_q \right) + \omega_f \tag{3}$$

where T_e is the electromagnetic torque, and p is the number of magnetic pole pairs. Accordingly, the mechanical equation of motion is formulated as follows:

$$J \frac{d\omega_m}{dt} = T_e - T_L - B\omega_m \tag{4}$$

where ω_m is the mechanical angular velocity, J is the moment of inertia, T_L is the load torque, and B is the viscous friction coefficient. For a surface-mounted PMSM, where $L_d = L_q$, the electromagnetic torque equation becomes:

$$T_e = \frac{3}{2} \times i_q \times p \times \varphi_f \tag{5}$$

3. Methods

Field-oriented control (FOC) is recognized as vector control and is a strategy utilized to control PMSM and induction motor (IM). FOC presents excellent control ability through the entire range of torque and speed. FOC modeling needs the conversion of stator current from the stationary reference frame to the d-q reference frame.

3.1. Field-oriented control (FOC)

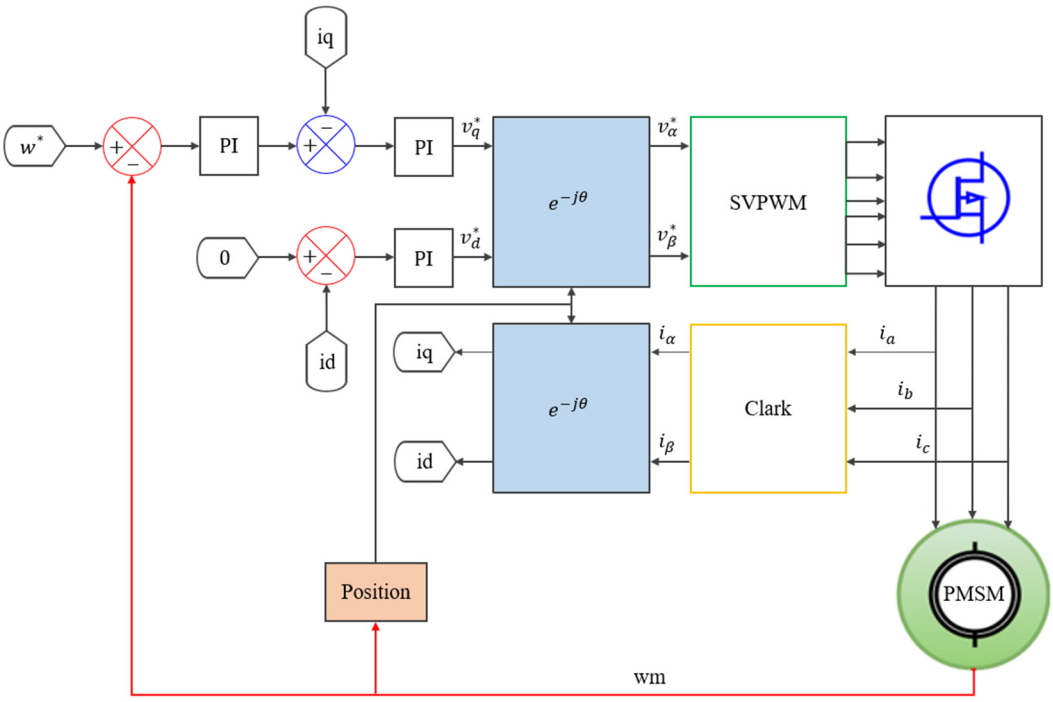

Fig. 1 Functional diagram of PMSM FOC based on PI

FOC is a method for variable-frequency drives with rotating magnetic field motors. Initially, vector control served as a control technology for three-phase asynchronous motors. However, given its simple principle and easy control method, it was widely used to control PMSM. FOC is to control the distribution of the stator and rotor magneto-motive force on the d-q axis system, thereby controlling the change of the motor torque and thereby achieving speed regulation of the motor [13]. A fixed

proportional relationship is present between the winding magnetomotive force and the winding current. Hence, vector control can be equivalent to controlling the current change to achieve motor control [14]. The core of vector control is to decouple the three-phase current through coordinate transformation and simplify the three-phase system into a two-phase system to simplify the control object. Therefore, the vector control technique is commonly used in the control of electric vehicles. PMSM closed-loop FOC can be built, and its schematic is displayed in Fig. 1.

3.2. Improvement of field-oriented control (FOC)

PI control is easy to implement and does not require precise mathematical models. It can also achieve a separate adjustment of the proportional and integral links. However, owing to the linear combination characteristics of PI control, a series of problems will arise in some environments with complex control mechanisms, such as significant overshoot, waveform oscillation, control lag, uncertainty, etc. This is also prominent in PMSMs [15]. Therefore, in response to the above problems, ADRC is adopted to address the issues of PI control in overshoot oscillation and other aspects. Based on the space vector pulse width modulation (SVPWM) of the three-phase PMSM, the PI controllers of the speed loop and the current loop are replaced by ADRC-based controllers to improve important index parameters such as overshoot, response speed, and recovery speed.

The current loop and speed loop controller modules built in this model, based on ADRC, are combined to construct a corresponding simulation and conduct simulation verification to test its robustness and response speed and compare it with PI control. Thus, PMSM closed-loop FOC can be built, and its schematic is presented in Fig. 2.

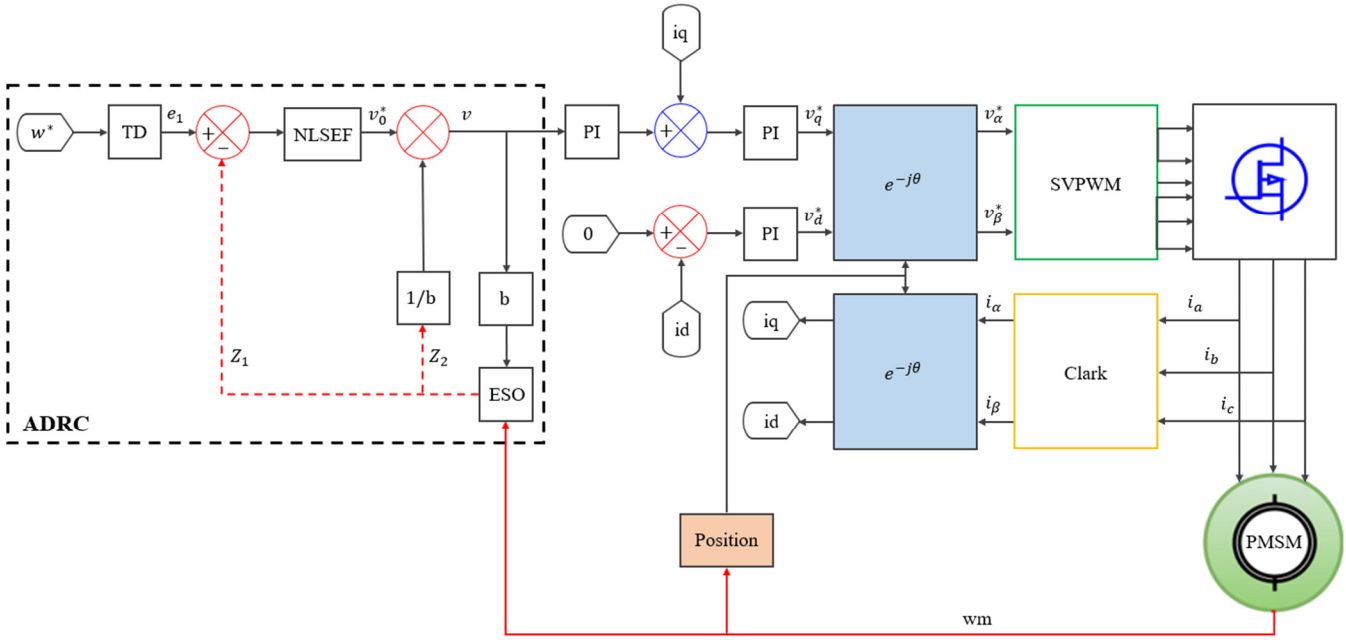

Fig. 2 Functional diagram of PMSM FOC based on ADRC

4. Principle and Composition of ADRC

Compared with classical proportional-integral-derivative (PID) control, ADRC needs to introduce some controlled information in the control process, such as the order of the controlled object, the "time scale" representing the speed of system change, etc. Simultaneously, it offers such as simplified algorithm implementation, fast response speed, and good anti-disturbance performance [16]. The extended state observer (ESO) first observes the state information of each feedback quantity and the disturbance error information while controlling the controlled object. It subsequently transmits the observed quantities from the ESO and the set reference quantity to the nonlinear control part for error calculation and disturbance compensation. Finally, the compensated information is transmitted to the controlled object, and the control performance is

improved through this process [17]. The ADRC is mainly composed of an arranged transition process known as the tracking differentiator (TD), an ESO, and a nonlinear state error feedback control rule (NLSEF). Its basic structural block illustration is presented in Fig. 3.

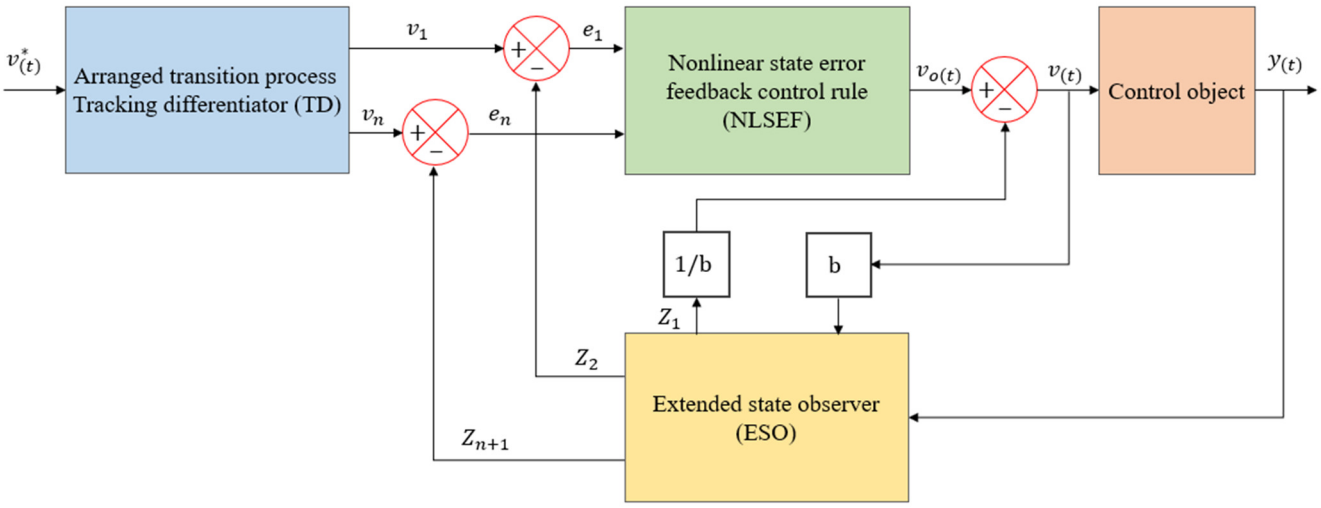

Fig. 3 Basic structure block of n-order ADRC

As shown in the figure, $v^*_{(t)}$ represents the assumed reference input, v_1 is the signal refined by the TD. Z_2 denotes the state observation feedback value enhanced by the ESO, and Z_1 represents the disturbance signal feedback value of the controlled system observed by the ESO. The values e_1 to e_n represent the error between the input reference value and the state observation feedback value [18]. As depicted in Fig. 3, the TD mainly differentiates the input reference value and arranges it reasonably to achieve a smoother signal input at the next level; the ESO mostly observes the disturbance signal and compensates for the required control quantity. In addition, since the feedback quantity is obtained by expanding the observed signal, high accuracy of the mathematical model is not required. The nonlinear feedback control law reasonably compensates for the error signal, thereby achieving better dynamic performance [19].

Now, for the design of the speed loop, the resulting speed equation can be derived, as shown below, by combining the electromagnetic torque equation in the numerical model of a PMSM with the motor motion equation.

$$\dot{\omega} = \frac{3 \times i_q \times p \times \varphi_f}{2J} - \frac{B}{J} \times \omega - \frac{T_L}{J} \tag{6}$$

If $F_{(\omega)} = -(B/J) \times \omega$, $b_0 = (3 \times p \times \varphi_f)/2J$, and $r_{s(t)} = -T_L/J$, the resulting expression can be written as follows:

$$\dot{\omega} = F_{(\omega)} + i_q \times b_0 + r_{s(t)} \tag{7}$$

In Eq. (7), $\gamma_{s(t)}$ can be regarded as a system disturbance. To enable compatibility between the ADRC and the speed model, $\gamma_{s(t)}$ can be substituted with a nonlinear function.

In the speed-loop anti-disturbance controller, the TD and the ESO are described by the following equations.

$$\begin{cases} E_{s0} = \dot{\omega} - v_{s1} \\ \dot{v}_{s1} = -r_{s0} \times fal\left(E_{s0}, \alpha_{s0}, \delta_{s0}\right) \end{cases} \tag{8}$$

$$\begin{cases} E_{s0} = z_{s1} - \omega \\ \dot{z}_{s1} = z_{s2} - \beta_{s1} \times fal\left(E_{s1}, \alpha_{s1}, \delta_{s1}\right) + F_{s(z_{s1})} + i^*_q \times b_0 \\ \dot{z}_{s2} = -\beta_{s2} \times fal\left(E_{s1}, \alpha_{s1}, \delta_{s1}\right) \end{cases} \tag{9}$$

In Eq. (8), E_{s0} represents the error between the speed reference value and the differential signal of the TD itself. This value is used as the nonlinear function input corresponding to the differential signal, and the speed signal is tracked by adjusting the gain coefficient reasonably; r_{s0} represents the adjustment gain value of the nonlinear function in the differential signal of the TD of the speed loop ADRC. In Eq. (9), E_{s1} represents the error between the speed signal estimated by the extended observer and the speed signal fed back, which will be used as the input signal corresponding to the nonlinear function in the ESO; β_{s1} and β_{s2} represent the gain coefficient corresponding to the differential component of the tracking signal and the gain coefficient of the disturbance error estimation, respectively. To analyze Eqs. (8) and (9) comprehensively, the simulation diagram of the TD and the ESO of the speed loop ADRC can be built. The block diagrams of the TD and the ESO of the speed loop ADRC are shown in Figs. 4 and 5, respectively.

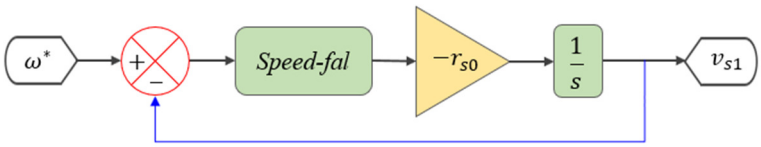

Fig. 4 Local diagram of speed loop ADRC TD

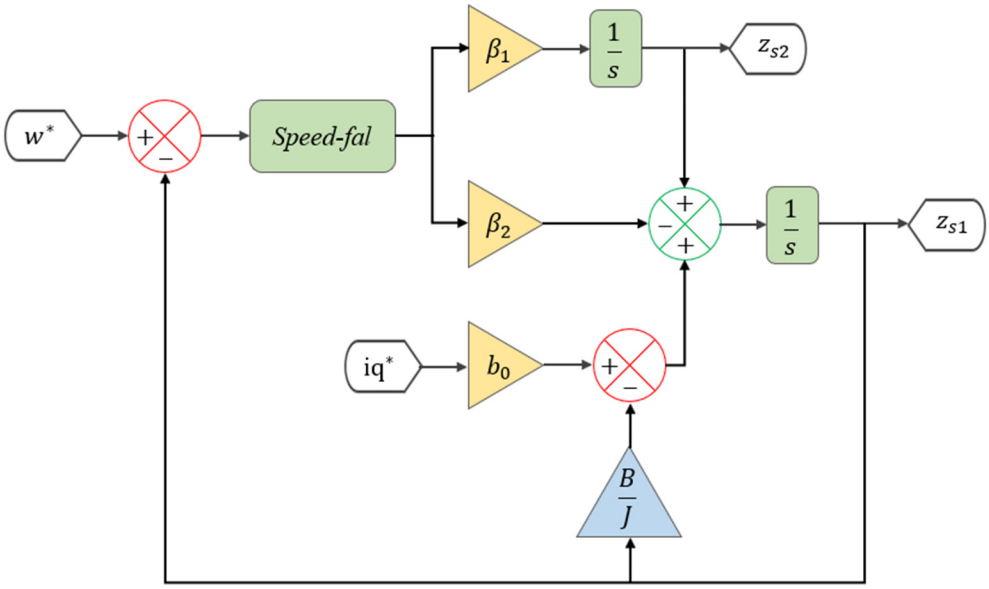

Fig. 5 Local diagram of speed loop ADRC ESO

In the nonlinear state error feedback control law, the characteristic curve of the nonlinear function *fal* is not smooth, and this non-smooth characteristic is prone to causing vibration. Simultaneously, this article pertains to a first-order control system, replacing the *fal* function in NLSEF with a suitable proportional gain. Simultaneously, as indicated in Eq. (6), the derivative of the speed is related to itself [20]. Therefore, in the speed loop equation, $(z_{s2} + fs(z_{s1}))/b_0$. It is used to compensate for the control law. The control law applied in the speed loop is given below.

$$\begin{cases} E_{s2} = v_{s1} - z_{s1} \\ i_{qo(t)} = k_s \times e_{s2} \\ i^*_{q(t)} = i_{qo(t)} - \dfrac{z_{s2} + F_{s(z_{s1})}}{b_0} \end{cases} \tag{10}$$

where k_s represents the gain coefficient of the control law, e_{s2} represents the error value between the tracking signal of the TD and the observation signal of the ESO, which is used as the controlled input of the control law and represents the compensation factor of the disturbance estimation feedback of the ESO. The simulation diagram of the speed-loop anti-disturbance control law is displayed in Fig. 6.

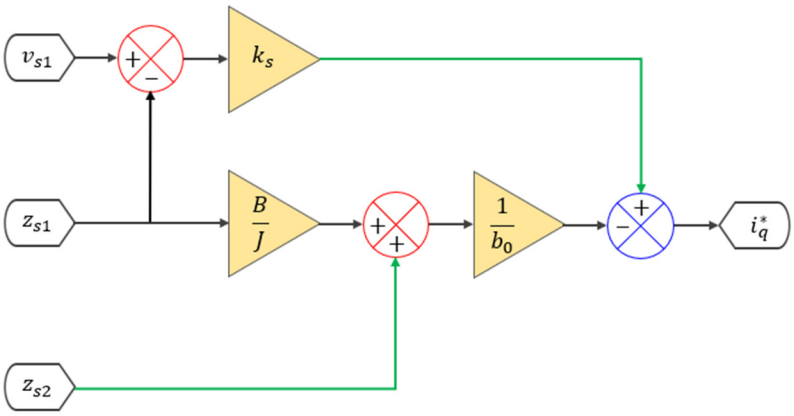

Fig. 6 Local diagram of speed loop ADRC control law

According to the PMSM speed control model, the PI controller of the speed loop in the FOC control algorithm is replaced by the ADRC controller. This reinforces the system's anti-disturbance dynamic monitoring performance. In other words, by introducing the proportional feedback method of speed monitoring error, the anti-disturbance capability of the system is further enhanced. The flowchart implementation process of the speed loop ADRC controller is shown in Fig. 7.

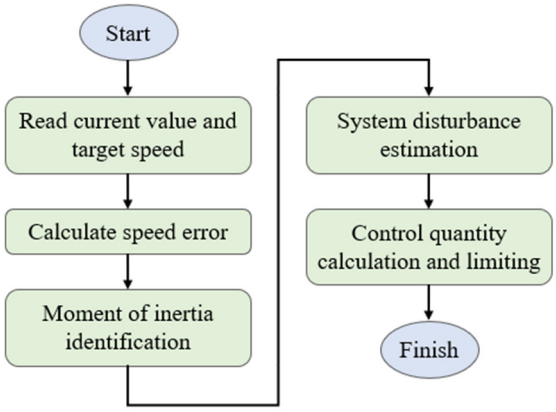

Fig. 7 ADRC controller flowchart

5. Discussion and Results

To verify the effectiveness of the suggested scheme for PMSM drive systems, a corresponding simulation model is built in the MATLAB/Simulink environment, and the proposed FOC based on ADRC is compared with the traditional FOC. The main parameters of the PMSM used are displayed in Table 1. Parameters selected by the speed loop ADRC are demonstrated in Table 2.

Table 1 Parameters of the PMSM

Parameter	Value
DC bus voltage	311 V
Rated speed	1,500 rpm
Rs	0.958 Ω
Ld	5.25 mH
Lq	12 mH
Flux	0.1827 wb
Pole	4

Table 2 Parameters of speed loop ADRC

Parameter	Value
$\alpha_{s0} = \alpha_{s1}$	0.95
$\delta_{s0} = \delta_{s1}$	0.01
r_{s0}	10,000
β_{s1}	45
β_{s2}	1,100
k_s	210
b_0	130

The corresponding speed information can be obtained according to the speed waveform in Fig. 8. The speed information shows the speed variations of the PMSM when starting under no-load conditions and when the load suddenly increases. In the case of no-load starting, the maximum speed rises to 1,265 r/min. After 0.16 s, the system enters a relatively stable operating

state, and Table 2 shows the rated speed by 0.25 s. When the system load suddenly increases by 10 N·m, the speed drops to a minimum of 1,179 r/min, and the time required to recover to the rated speed is approximately 0.28 s. According to the simulation results, although PI control has a simple structure, it exhibits significant speed overshoot under no-load starting conditions and requires a relatively long adjustment time. In addition, its anti-interference capability is weak, the recovery from load disturbance is slow, and its response speed and tracking performance are poor.

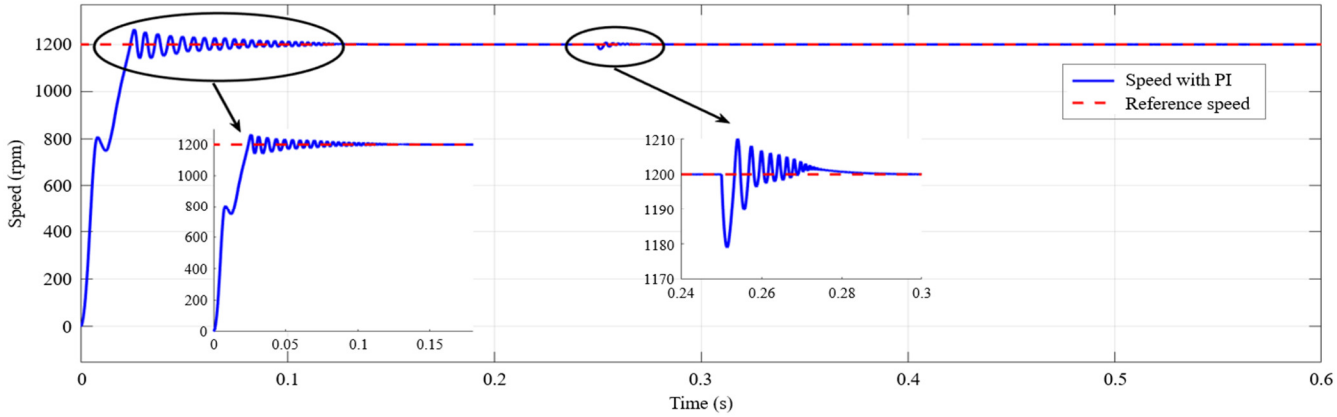

Fig. 8 Speed curve of PMSM FOC based on PI

The corresponding speed information can be obtained according to the speed waveform in Fig. 9. The speed information shows that when the speed loop adopts the ADRC, the speed of the PMSM changes when starting under no-load conditions, and the speed changes when the load suddenly increases. When the speed loop ADRC control strategy is adopted, the maximum speed increases to 1,218 r/min within 0.04 s under no-load starting conditions and reaches a stable state at the rated speed of 0.25 s. When the system load suddenly increases by 10 N·m, the speed drops to a minimum of 1,177 r/min, and the time required to recover to the rated speed is approximately 0.26 s.

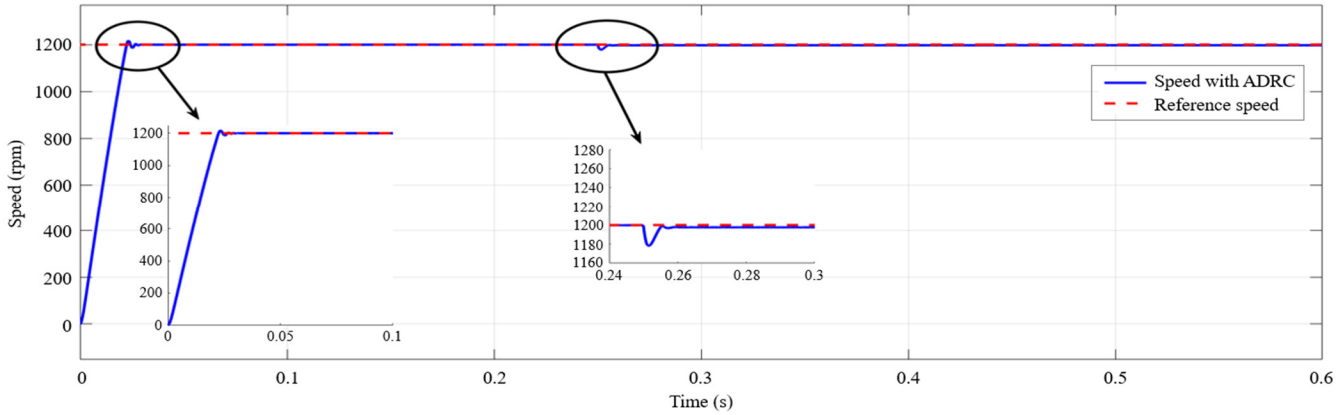

Fig. 9 Speed curve of PMSM FOC based on ADRC

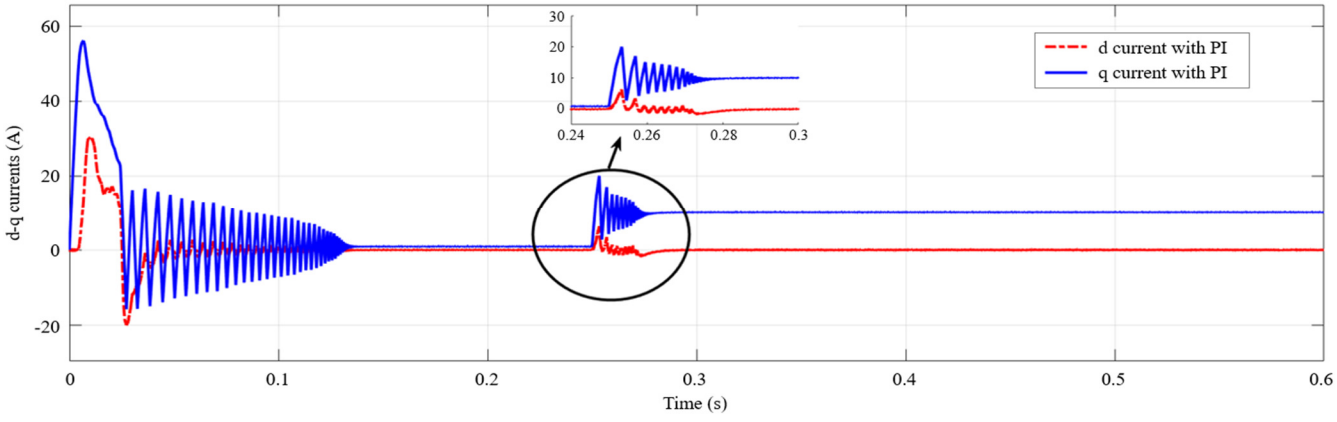

Fig. 10 q-d currents based on PI

As depicted in Fig. 10, which shows the q-d axis current. The control strategy with PI exhibits relatively large current fluctuations when the motor starts with no burden load at t = 0 and undergoes in torque increase at t = 0.25 s. In contrast, as shown in Fig. 11, the control strategy with ADRC results in relatively smaller current fluctuations under the same conditions.

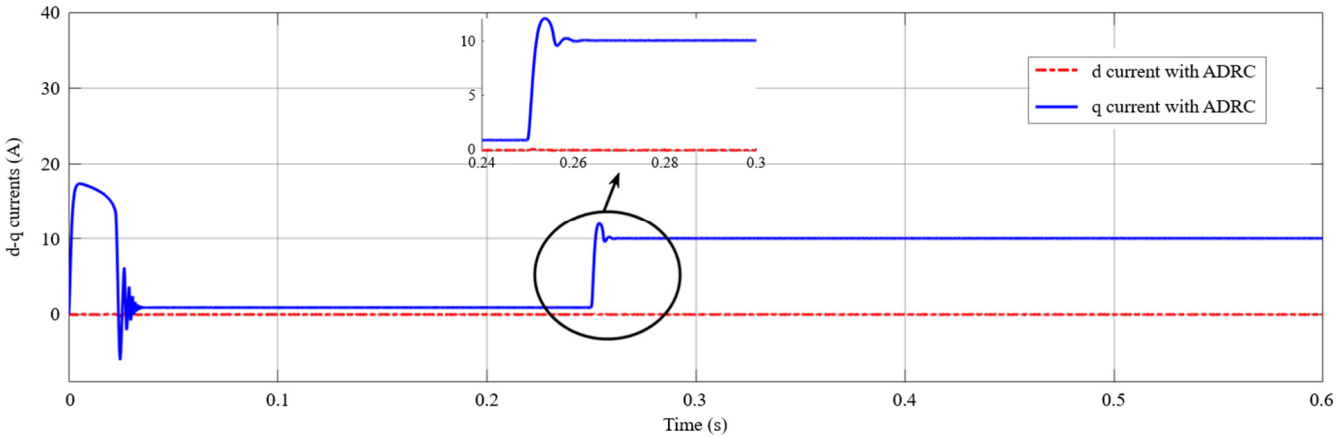

Fig. 11 q-d currents based on ADRC

As shown in Fig. 12, under steady-state operation without sudden load application, the current fluctuates approximately between −1.02 A and 1.02 A, following a roughly sinusoidal pattern. After reaching a stable state, the fluctuation range increases to about −10.12 A to 10.12 A. Fig. 13 presents the responses of the three-phase currents under the ADRC control strategy when a load torque is suddenly applied at t = 0.25 s. In steady-state operation without load disturbance, the current fluctuates approximately between −0.9 A and 0.9 A, in a sinusoidal form. After the system stabilizes, the fluctuation range extends to around −9.9 A to 9.9 A.

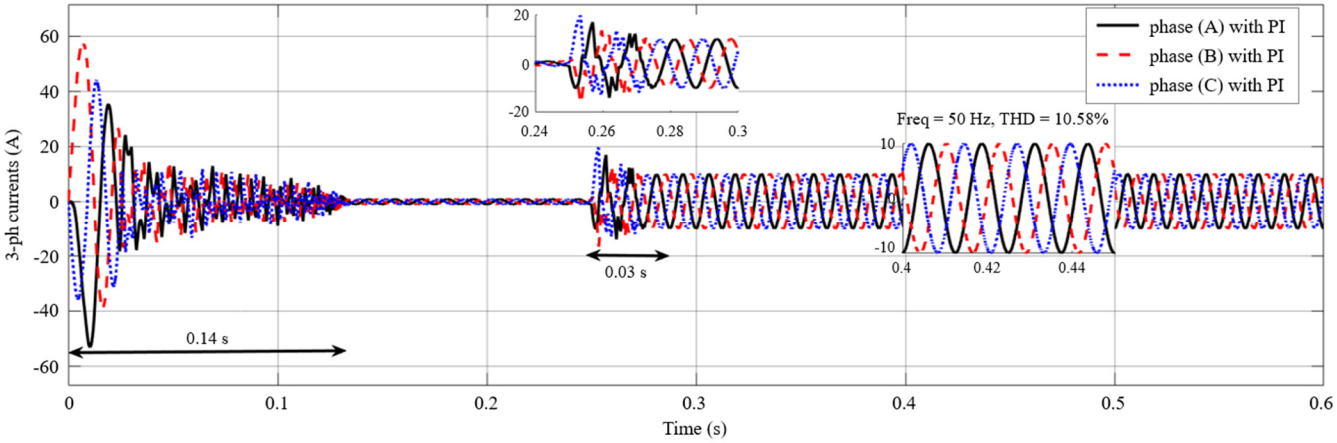

Fig. 12 Stator three-phase (A, B, C) currents based on PI

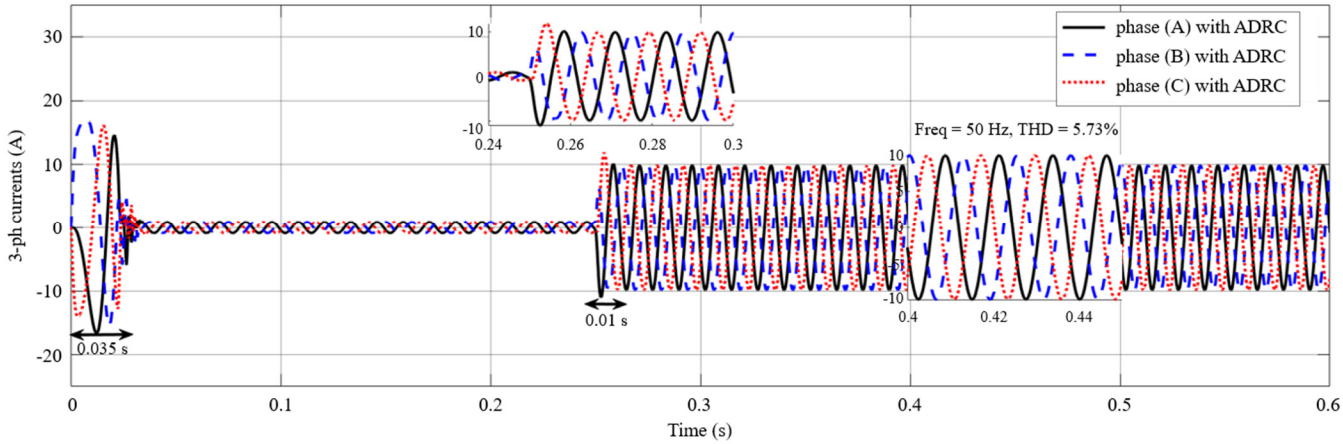

Fig. 13 Stator three-phase (A, B, C) currents based on ADRC

Fig. 14 depicts the current errors between the reference and measured currents for each phase under the PI-based control strategy. The error observed for phase A ranges from 52.99 to −38.92, for phase B from 40.8 to −58.28, and for phase C from 37.06 to −44.59. Fig. 15 presents the current errors between the reference and measured currents for each phase under the ADRC-based control strategy. The error observed for phase A ranges from 19.9 to −19.59, for phase B from 19.9 to −23.19), and for phase C from 19.9 to −19.64.

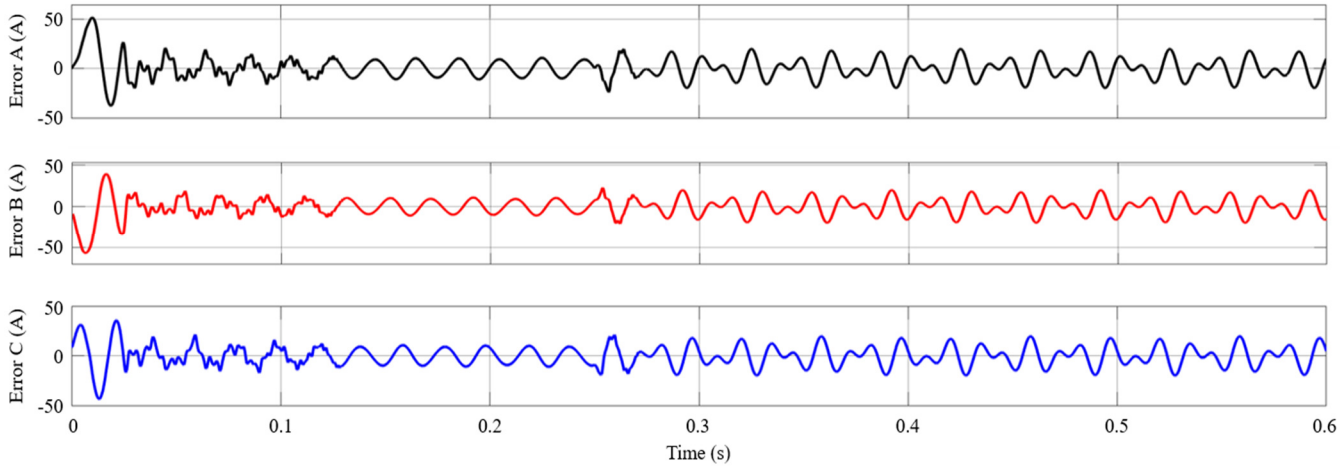

Fig. 14 Current Error based on PI

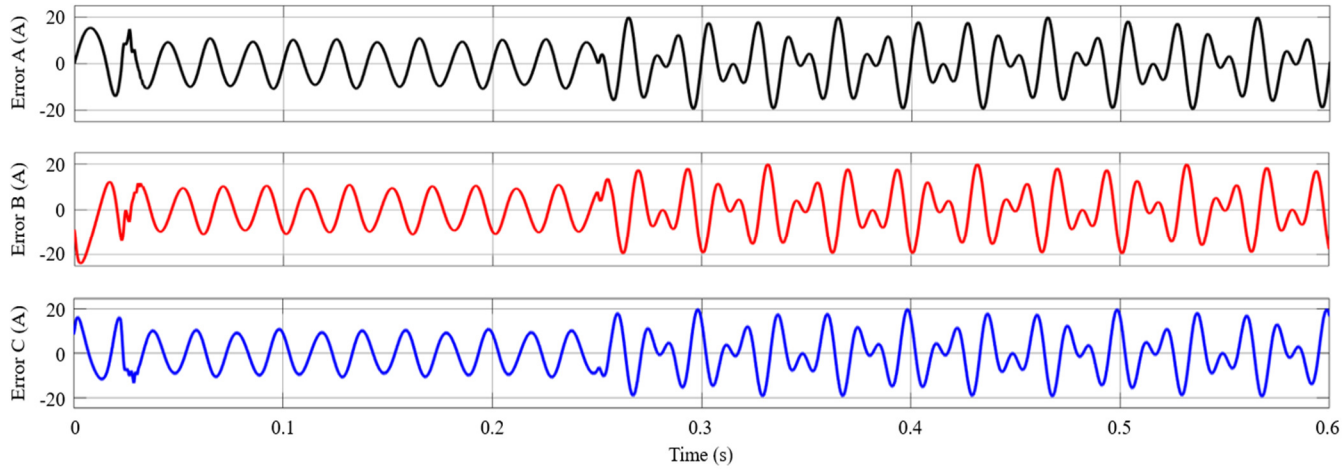

Fig. 15 Current Error based on ADRC

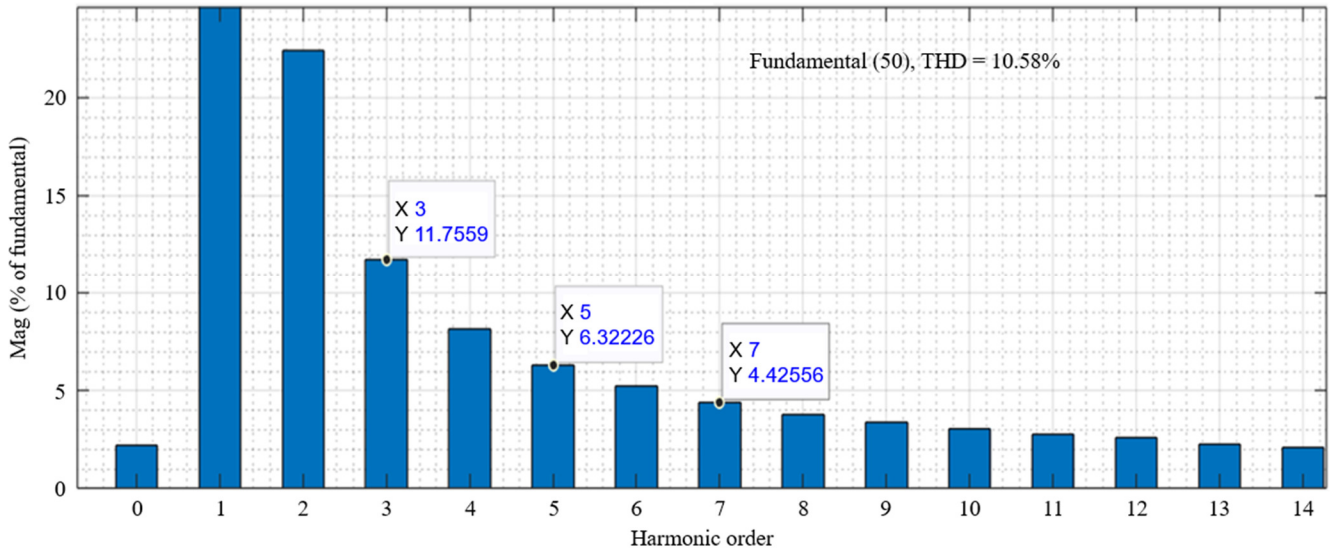

Fig. 16 THD and spectrum analysis of stator current with PI

The comparative analysis in Figs. 16 and 17 show that the THD of the current and the amplitude of the fundamental frequency component are 10.58% and 5.73%, respectively, under the PI-based control strategy. By contrast, the ADRC-based strategy significantly improves the current spectrum by reducing harmonic distortion. In the harmonic content analysis of the PMSM phase currents, the 3rd, 5th, and 7th harmonics exhibit the highest amplitudes under PI control, which are effectively suppressed when ADRC is applied.

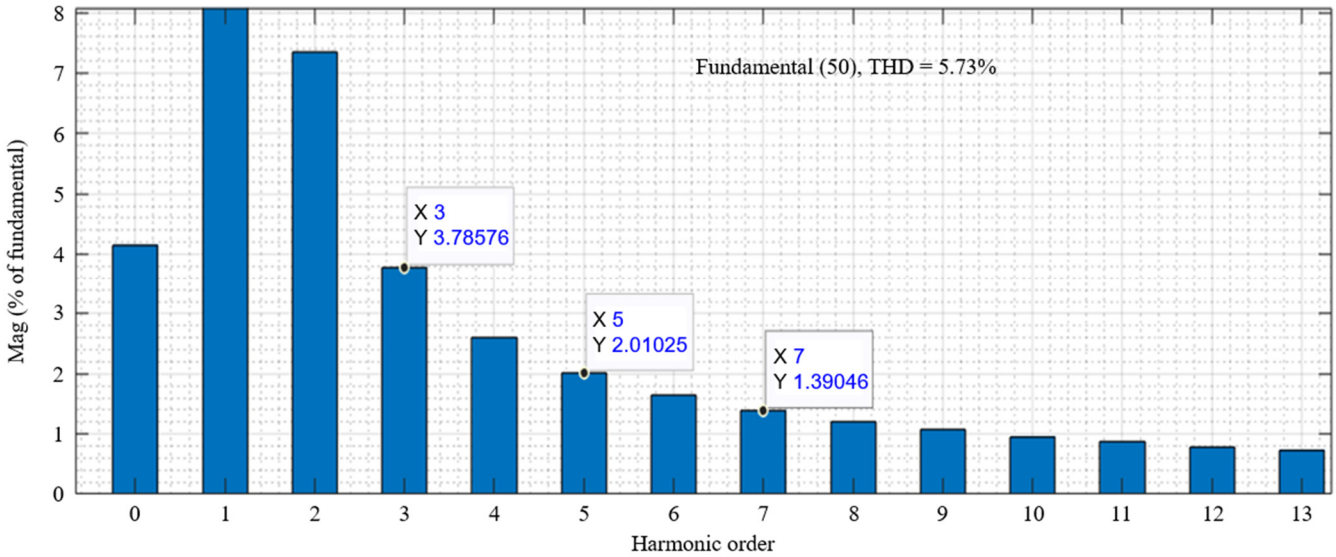

Fig. 17 THD and spectrum analysis of stator current with ADRC

Figs. 16 and 17 display and compare the simulation results of the traditional PI and ADRC control strategies. A summary of the specific data is provided in Table 3. Meanwhile, Table 4 presents a comparison between the proposed method and other related approaches in the literature. The ADRC technique for electric motor control systems has proven effective in enhancing system flexibility, response time, and tracking performance.

Table 3 shows a comparison between FOC based on pi and FOC based on ADRC

Results	FOC based on PI		FOC based on ADRC
Speed response time	0.14 s		0.04 s
Current response time	0.03 s		0.01 s
Overshoot for three-phase current at change load	19.65		11.82
Overshoot for q-d currents at change load	q	20.05	12.07
	d	6.34	0.15
THD	10.58%		5.73%

Table 4 compares the proposed method and other references.

Ref.	Method	Speed response time	q-d currents
This study	FOC based on ADRC	0.04 s	Overshoot less
Zhou et al. [21]	ADRC	0.0458 s	-
Luo et al. [22]	ADRC + FOPID	More than	More than

6. Conclusions

This paper proposed an ADRC strategy for electric motor control systems to enhance system resilience, response time, and tracking performance. To validate the effectiveness of the proposed method, simulation models of the traditional PI-based and ADRC-based speed regulation systems were developed based on a three-phase PMSM. Comparative simulation analyses were conducted to evaluate the speed-tracking capability, adaptability, anti-interference performance, and harmonic distortion. The main conclusions are summarized as follows:

(1) The ADRC-based system demonstrates superior speed-tracking capability compared to the conventional PI-based system.

(2) The ADRC-based controller provides better adaptability, stronger anti-interference ability, and faster dynamic response.

(3) The ADRC-based controller significantly reduces total harmonic distortion (THD), achieving 5.73%, compared to 10.58% with the PI-based controller.

Conflicts of Interest

The authors declare no conflict of interest.

References

[1] X. Lin, W. Huang, W. Jiang, Y. Zhao, and S. Zhu, "A Stator Flux Observer with Phase Self-Tuning for Direct Torque Control of Permanent Magnet Synchronous Motor," IEEE Transactions on Power Electronics, vol. 35, no. 6, pp. 6140-6152, 2020.

[2] S. T. Bahar and R. G. Omar, "Permanent Magnet Synchronous Motor Torque Ripple Reduction Using Predictive Torque Control," Journal of Engineering and Sustainable Development, vol. 27, no. 3, pp. 394-406, 2023.

[3] M. Amirkhani and M. Mirsalim, "A Comprehensive Analysis of a Complementary-Rotor Doubly Salient Permanent Magnet Motor for High Torque Applications," 12th Power Electronics, Drive Systems, and Technologies Conference, pp. 1-5, 2021.

[4] Y. Pu, Z. Xiang, M. Jiang, and X. Zhu, "Investigation on Electromagnetic Torque of a Flux-Switching Permanent Magnet Motor from Perspective of Flux Density Harmonic Reduction Ratio," IEEE Transactions on Magnetics, vol. 58, no. 2, article no. 8101706, 2022.

[5] S. T. Bahar and Y. G. Rashid, "A Study on an MPPT Control Approach Using Artificial Intelligence and the Perturb and Observe Method," Diyala Journal of Engineering Sciences, vol. 17, no. 2, pp. 131-143, 2024.

[6] M. Vidlak, L. Gorel, and P. Makys, "Performance Evaluation, Analysis, and Comparison of the Back-EMF-Based Sensorless FOC and Stable V/f control for PMSM," International Symposium on Power Electronics, Electrical Drives, Automation and Motion, pp. 318-323, 2022.

[7] Z. Ruan, W. Song, L. Zhao, Y. Zhang, and Y. Guo, "A Variable Switching Frequency Space Vector Pulse Width Modulation Control Strategy of Induction Motor Drive System with Torque Ripple Prediction," IEEE Transactions on Energy Conversion, vol. 38, no. 2, pp. 993-1003, 2023.

[8] S. A. Saleh and A. Rubaai, "Extending the Frame-Angle-Based Direct Torque Control of PMSM Drives to Low-Speed Operation," IEEE Transactions on Industry Applications, vol. 55, no. 3, pp. 3138-3150, 2019.

[9] S. T. Bahar and R. G. Omar, "Torque Ripple Alleviation of a Five-Phase Permanent Magnet Synchronous Motor Using Predictive Torque Control Method," International Journal of Power Electronics and Drive Systems, vol. 13, no. 4, pp. 2207-2215, 2022.

[10] C. Miguel-Espinar, D. Heredero-Peris, R. Villafafila-Robles, and D. Montesinos-Miracle, "Review of Flux-Weakening Algorithms to Extend the Speed Range in Electric Vehicle Applications with Permanent Magnet Synchronous Machines," IEEE Access, vol. 11, pp. 22961-22981, 2023.

[11] H. Wu, W. Zhao, Z. Li, and X. Wang, "Torque Improvement of Spoke-Type Permanent Magnet Motor with Auxiliary Stator Using Harmonic Current Control Strategy," CES Transactions on Electrical Machines and Systems, vol. 7, no. 2, pp. 210-217, 2023.

[12] S. T. Bahar and D. R. Neama, "Improved Direct Torque Control Utilizing Model Predictive Control Approach for Permanent Magnet Synchronous Motor", Al-Iraqia Journal for Scientific Engineering Research, vol. 3, no. 2, pp. 57-64, 2024.

[13] H. Xie, F. Wang, Y. He, J. Rodríguez, and R. Kennel, "Encoderless Parallel Predictive Torque Control for Induction Machine Using a Robust Model Reference Adaptive System," IEEE Transactions on Energy Conversion, vol. 37, no. 1, pp. 232-242, 2022.

[14] Z. Zhang, Y. Liu, X. Liang, H. Guo, and X. Zhuang, "Robust Model Predictive Current Control of PMSM Based on Nonlinear Extended State Observer," IEEE Journal of Emerging and Selected Topics in Power Electronics, vol. 11, no. 1, pp. 862-873, 2023.

[15] W. Zhang, H. Zhu, Y. Xu, and M. Wu, "Direct Control of Bearingless Permanent Magnet Slice Motor Based on Active Disturbance Rejection Control," IEEE Transactions on Applied Superconductivity, vol. 30, no. 4, pp. 1-5, 2020.

[16] L. Zhu, G. Zhang, R. Jing, G. Bi, R. Xiang, G. Wang, et al., "Nonlinear Active Disturbance Rejection Control Strategy for Permanent Magnet Synchronous Motor Drives," IEEE Transactions on Energy Conversion, vol. 37, no. 3, pp. 2119-2129, 2022.

[17] J. Xu, Z. Wei, and S. Wang, "Active Disturbance Rejection Repetitive Control for Current Harmonic Suppression of PMSM," IEEE Transactions on Power Electronics, vol. 38, no. 11, pp. 14423-14437, 2023.

[18] S. Lin, Y. Cao, C. Li, Z. Wang, T. Shi, and C. Xia, "Two-Degree-of-Freedom Active Disturbance Rejection Current Control for Permanent Magnet Synchronous Motors," IEEE Transactions on Power Electronics, vol. 38, no. 3, pp. 3640-3652, 2023.

[19] J. Li, H. Ren, S. Wang, and Y. Fang, "Integral Sliding Mode Control for PMSM with Uncertainties and Disturbances via Nonlinear Disturbance Observer," 39th Chinese Control Conference, pp. 2055-2060, 2020.

[20] Z. Gong, C. Zhang, X. Ba, and Y. Guo, "Improved Deadbeat Predictive Current Control of Permanent Magnet Synchronous Motor Using a Novel Stator Current and Disturbance Observer," IEEE Access, vol. 9, pp. 142815-142826, 2021,

[21] K. Zhou, M. Ai, Y. Sun, X. Wu, and Ran Li. "PMSM Vector Control Strategy Based on Active Disturbance Rejection Controller," Energies, vol. 12, no. 20, article no. 3827, 2019.

[22] J. Luo, L. Wang, and B. Liu, "Low-Speed Control of PMSM Based on ADRC + FOPID," Systems Science & Control Engineering, vol. 9, no. 1. pp. 73-87, 2021.